PHYSICAL REVIEW B VOLUME 15, NUMBER 1 1 JANUARY 1977

Low-spin high-spin equilibria in 1T-$Fe_xTa_{1-x}S_2$ ($x \leq 1/3$) and the temperature dependence of the associated energy gap

M. Eibschütz, M. E. Lines, and F. J. DiSalvo
Bell Laboratories, Murray Hill, New Jersey 07974
(Received 1 July 1976)

Measurements of magnetic susceptibility and Mössbauer isomer shift are reported for 1T-$Fe_xTa_{1-x}S_2$ ($x \leq 1/3$) and indicate the existence of a gradual transition from low-spin to high-spin Fe^{2+} as a function of increasing temperature. A quantitative analysis of the data reveals that the energy gap between the ground $^1A_1$ state and the lowest of the spin orbitally split $^5T_2$ levels is temperature dependent. The detailed behavior, which is dependent on concentration x, can be quantitatively understood in terms of a modulation of the cubic crystal field and Hund's-rule exchange energies by the motion of the local ligand environment and includes important contributions both from a static striction mechanism and from the thermal excitation of the relevant local mode.

I. INTRODUCTION

Because of the comparable magnitude of cubic-crystal-field splitting and Hund's-rule exchange in certain magnetic materials containing 3d transition-metal ions, transitions between low-spin and high-spin levels have long been anticipated and indeed observed in several situations.[1-6] The basic mechanism of such a low-spin (LS) high-spin (HS) transition has been outlined by Bari and Sivardière[7] (following earlier work by Chestnut[8]) and, in the simplest case of effectively isolated magnetic ions, takes the form of a coupling between the magnetic properties and a local lattice distortion. For Fe^{2+} ($3d^6$) the relevant states are LS $^1A_1(t_2^6)$, a singlet, and HS $^5T_2(t_2^4e^2)$ with 15 levels split by spin-orbit coupling and lower-symmetry crystal field. The most dramatic effects as a function of temperature are seen when the singlet is lowest, and Bari and Sivardière find for this situation that the resulting transition may be sharp (actually first order) if the coupling to the lattice is strong enough, or "continuous." In the latter case the "transition" occurs as a function of increasing temperature in a statistical sense only via a thermal population of the higher-degeneracy HS levels, although the coupling to the lattice is still important and manifests itself as a thermal modulation of the LS-HS energy gap.

In this paper we describe the first observation of a continuous LS-HS transition in Fe^{2+} and the first detailed observation and quantitative theoretical explanation of the temperature dependence of a LS-HS energy gap (preliminary reports of this work have been given in Refs. 9 and 10). We have carried out measurements of magnetic susceptibility and Mössbauer isomer shift in the substitutionally iron-doped layer chalcogenide material 1T-$Fe_xTa_{1-x}S_2$ for several different concentration levels up to $x=\frac{1}{3}$, and have established that the iron enters exclusively as Fe^{2+} and undergoes a continuous LS-HS transition between ~200 and ~500 °K, with the detailed behavior depending on concentration. A careful analysis of the data using a statistical model with a LS-HS energy gap E_g between the $^1A_1$ ground state and the lowest of the $^5T_2$ levels reveals that E_g is temperature dependent, and we are able to ascertain the detailed form of this temperature dependence for a series of concentrations x. By extending the theory of Bari and Sivardière to include spin-orbit coupling within the $^5T_2$ levels and the dynamic as well as static effects of local ligand vibrations on the striction process, we are able to provide an essentially quantitative understanding of the temperature dependence of the gap for each x and thereby to confirm the physical origin of the effect.

The paper is organized as follows: Following the Introduction, the sample preparations and our experimental techniques are described in Sec. II. In Sec. III we present and analyze our susceptibility and Mössbauer spectra. Since the nominally pure 1T-TaS_2 is metallic at high temperatures and exhibits charge-density-wave instabilities at lower temperatures,[11] no quantitative magnetic analysis of the iron-substituted material can begin until the role played by conduction electrons (e.g., Pauli paramagnetism) and the proper characterization of the iron valence state is accomplished. This is described in Sec. IV, where it is established that the conduction electrons play no significant magnetic role for concentrations $x \gtrsim 0.1$ and that the iron is essentially 100% Fe^{2+} at our temperatures of interest. Section V describes the formal LS-HS statistical theory for Fe^{2+} with an energy gap E_g which is carried through simply as a temperature-dependent pa-

rameter to be determined by quantitatively fitting the susceptibility and Mössbauer data. The actual analysis of the data and determination of the precise temperature dependence of E_g for each x is described in Sec. VI. Finally, in Sec. VII the "striction" mechanism by which the cubic crystal field and Hund's-rule energy are modulated by ligand motion is detailed and the resulting theory used to fit the derived $E_g(T)$ curves for each x.

II. EXPERIMENT

$1T$-$Fe_xTa_{1-x}S_2$ ($x \leq \frac{1}{3}$) was prepared from stoichiometric mixtures of Ta, Fe (or Fe^{57}), and S sealed in a small quartz tube under vacuum (10 mTorr or less) and reacted initially for several days at 800 °C. After this initial reaction, the samples were opened, ground, pressed into pellets at 50 000 psi, and resealed in the quartz tube with enough excess sulfur to give approximately 1–2 atm vapor pressure at 900 °C (i.e., 1–2 mg/cm^3 of internal tube volume). These samples were reheated to 950 °C for 7 d, so that diffusion of the cations could occur producing essentially homogeneous pellets. The technique is described elsewhere.[12,13] Single crystals were prepared by iodine vapor transport [≈ 5 mg I/cm^3] in closed quartz tubes usually 16 mm i.d. and 200 mm long.[12] Again, for crystal growths, excess sulfur (1–2 mg/cm^3) is added to the transport tube. The growth temperature was ~700 °C. The temperature gradient between the (hotter) starting powder and the growth zone was between 50 and 100 °C. Complete transport occurred in 7–10 d, after which the tubes were rapidly quenched in cold water to ensure retention of the $1T$ phase. X-ray diffraction confirmed the presence of the $1T$ phase An additional confirmation of the pure-$1T$ crystal phase was provided by the fact that the smooth basal plane surfaces cleaved easily parallel to the layers and had the proper color (yellow bronze). X-ray fluorescence verified that the Fe was indeed included in the crystal in the desired level.

$1T$-$Fe_xTa_{1-x}S_2$ has the CdI_2 structure[14,15] [neglecting small distortions due to the charge-density wave (CDW)] which is the stable structure to at least 800 °C when $x \geq 0.02$. X-ray and electron-diffraction studies indicate that the Fe is randomly (or almost so) distributed on Ta sites; no evidence of Fe ordering is seen at any $x \leq \frac{1}{3}$. 200-KV transmission-electron-diffraction studies clearly show the existence of a CDW[11] in these compounds at room temperature for $x \leq 0.10$; at $0.15 \leq x \leq \frac{1}{3}$ diffuse scattering is observed but no sharp satellite peaks are seen that would indicate a CDW with a long coherence.[13] It is possible that in the latter range of x the CDW is not the ground state of the system, but that local distortions[16] or even short-range Fe order account for the diffuse scattering.

Magnetic susceptibility (χ) was measured on powder samples from 4.2 to 800 °K using a Faraday technique.[13] The absolute accuracy of the susceptibility compared to several standards is ±2%. The ^{57}Fe Mössbauer-effect (ME) spectra were obtained in a standard transmission geometry with a conventional constant-acceleration spectrometer.[17] The ME spectra were taken between 4.2 and 820 °K. Temperatures of 4.2 and 77.4 °K were obtained with the sample holder measured in a cryogenic liquid. Temperatures between 90 and 300 °K were obtained with the sample holder mounted in a Dewar vacuum space on a "cold finger" connected to the liquid reservoir by a thermal resistance. In the latter case the temperature was measured by a platinum resistance thermometer. A germanium resistance thermometer was used as a sensor for an automatic temperature controller which controlled the current to a heater on the cold finger. We estimate that our platinum resistor provided a measure of the average sample temperature accurate to ±0.5 °K. More details are described elsewhere.[18] A radiation-shield-insulated vacuum furnace was used for high-temperature measurements.[19] A Pt-Pt (10% Rh) thermocouple was used for our commercial automatic temperature controller. The temperature was measured by a second Pt-Pt (10% Rh) thermocouple. We estimate that the average sample temperature was accurate to ±1 °K.

III. RESULTS AND PRELIMINARY ANALYSIS

The magnetic susceptibility per mole of Fe (χ_m) is shown in Fig. 1 for powder samples at different x. The data in Fig. 1 have been corrected by subtracting a small Curie contribution at low T (which increases as $1/T$). Further, only changes from the low-temperature diamagnetic state are shown. Also, we do not attempt to correct at this moment for a temperature-dependent Pauli susceptibility that is seen in the nonmagnetic analog[13] $1T$-$Ti_xTa_{1-x}S_2$—but this should be 15% or less of the total χ at 900 °K and $x = 0.05$, and proportionally smaller at larger x. We return to this point later.

The data clearly show that Fe has no magnetic moment at low temperatures, but that at high temperatures a moment appears, which for low x roughly approaches the Curie χ_m expected for a spin state ($S = 2$, $g = 2$). At high temperatures there is a change in behavior when $x \geq 0.15$, in that χ_m approaches the same value independent

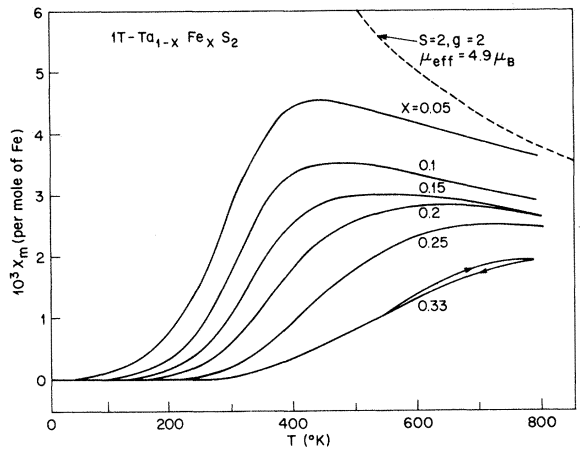

FIG. 1. Magnetic susceptibility per mole of Fe (χ_m) for $1T$-$Fe_xTa_{1-x}S_2$ powder ($0.05 \leq x \leq \frac{1}{3}$) versus temperature.

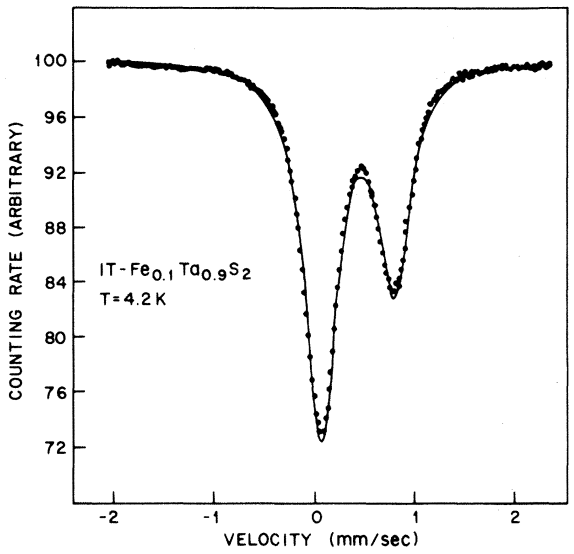

FIG. 2. Mössbauer absorption spectrum of $Fe_{0.1}Ta_{0.9}S_2$ at 4.2 °K. The solid line represents the sum of two Lorentzian least-squares fits to the data.

of x. Only at $x=\frac{1}{3}$ were small thermal hysteresis effects observed (as shown).

The ME absorption spectra for $1T$-$Fe_xTa_{1-x}S_2$ were taken in a mosaic of single crystals oriented with the c crystallographic axis parallel to the γ rays. For $x=0.1$ an enriched sample in ^{57}Fe has been used. The ^{57}Fe metal has been obtained by reducing $^{57}Fe_2O_3$ at 1000 °C in flowing hydrogen. A characteristic low-temperature ME spectrum for $x=0.1$ is shown in Fig. 2; examples of ME spectra in the transition region are shown in Fig. 3. Representative examples of the ME absorbtion spectra for $x=\frac{1}{3}$ at 4.2 °K and above room temperatures are shown, respectively, in Fig. 4 and 5. A least-squares fit to a sum of two Lorentzian curves is shown in Figs. 2–5 by the solid lines.

The two resonance lines observed in every spectrum are due to quadrupole splitting. At room temperature $\frac{1}{2}e^2qQ = -0.57 \pm 0.01$ and -0.66 ± 0.01 mm/sec for $x=0.1$ and $x=\frac{1}{3}$, respectively. At 4.2 °K, $\frac{1}{2}e^2qQ = -0.73 \pm 0.01$ mm/sec for both x. The linewidth is broad. At room temperature for $x=0.1$ the low-velocity ME linewidth is about 30% larger than that of the high-velocity one. The average full width at half-maximum (FWHM) is 0.38 ± 0.01 mm/sec for the low-velocity ME line. For $x=\frac{1}{3}$ the linewidth of the ME lines is about the same. At room temperature the FWHM is 0.33 ± 0.01 mm/sec. The room-temperature relative intensity (area ratio) of the lines is 1:2.35 instead of the theoretically expected 1:3, and may be due to misorientation of the mosaic of the single-crystal platelets, saturation effects, or the fact that the local symmetry may be no longer exactly axial symmetric due to the presence of incommensurate charge density waves.

The center shift (measured by the center of the one spectrum) as a function of temperature for $1T$-$Fe_{0.1}Ta_{0.9}S_2$ and $Fe_{1/3}Ta_{2/3}S_2$ is shown in Fig. 6. The magnitude of the isomer shift (0.63 ± 0.01 mm/sec) at 4.2 °K is the largest reported for ^{57}Fe in a low spin state ($^1A_1$).[20] This indicates a high degree of covalency in these metals. The center shift as a function of temperature has an "anomalous" behavior. The center shift as a function of concentration is also different from that expected. The χ and center-shift data show (as we shall demonstrate later on) a gradual transition from low-spin to high-spin Fe^{2+} with increasing temperature.

At low temperatures one set of Mössbauer lines has been observed. Again in the transition range 200–500 °K, only one set of ME lines is seen, with less than 10% difference in linewidth as compared to above or below this region; that is the maximum possible increase in linewidth is ≈ 0.03 mm/sec, which is much smaller than the difference of the (extrapolated) low-temperature and high-temperature center shift (δ_S) (0.15 mm/sec). This shows that the transformation is dynamic, the Fe atoms in the transition regime fluctuating between the low- and high-spin states faster than the inverse of the spectral splittings involved of 10^{-7} sec. Low-spin–high-spin transitions of Fe^{2+} have been previously observed, primarily in organometallic complexes.[6] In those cases two separate static Fe sites exist in the transition region; i.e., two sets of Mössbauer lines are seen, the intensity

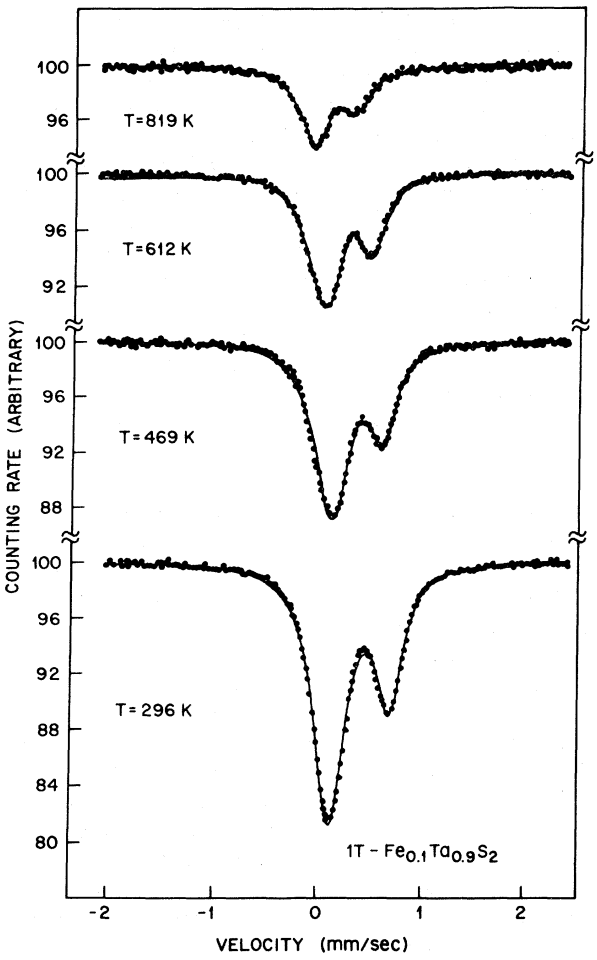

FIG. 3. Examples of ^{57}Fe Mössbauer absorption spectra of $1T$-$Fe_xTa_{1-x}S_2$ in the transition region. The solid lines are obtained by least-squares fits of the data to sums of two Lorentzian curves.

of one set growing while the other decreases. In $1T$-$Fe_xTa_{1-x}S_2$ each Fe atom must rapidly change its electronic state in the transition region so that the Mössbauer spectrum is time averaged and only one set of resonance lines is seen. This unusual behavior of the χ and δ_S data as a function of temperature and concentration will be discussed in the following sections.

IV. MAGNETIC SUSCEPTIBILITY—GENERAL OBSERVATIONS

The powder susceptibility data of Fig. 1 clearly show the absence of a magnetic moment at low temperatures for all concentrations x. This can only realistically be interpreted in terms of the existence of a singlet ground state for each Fe ion separately. The only other possibility would be in terms of a clustering of iron atoms into small even (but not odd) antiferromagnetic clusters—a

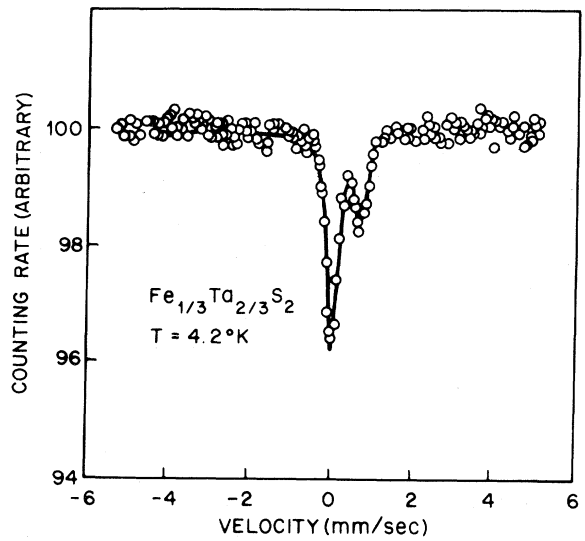

FIG. 4. Mössbauer absorption spectrum of $1T$-$Fe_{1/3}Ta_{2/3}S_2$ at 4.2 °K.

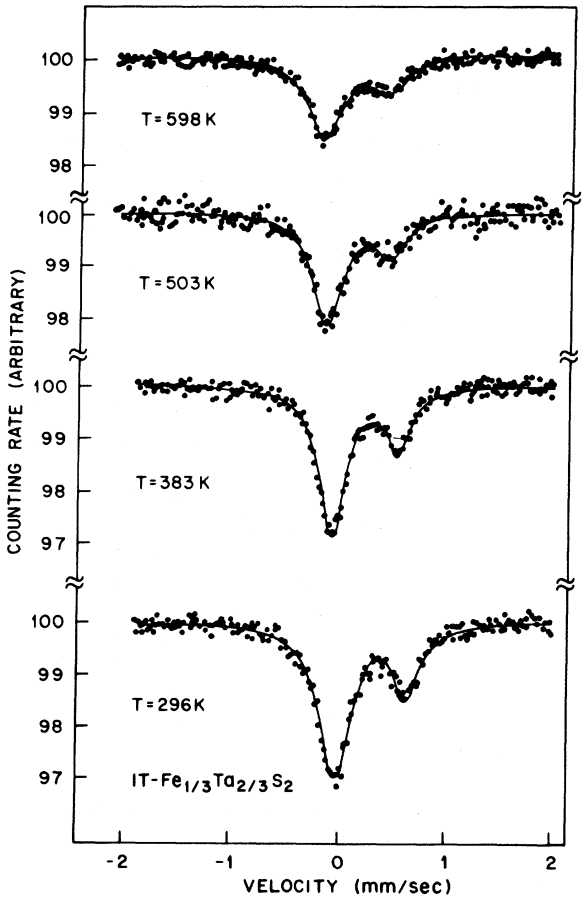

FIG. 5. Mössbauer absorption spectra of $1T$-$Fe_{1/3}Ta_{2/3}S_2$ below and in the transition region.

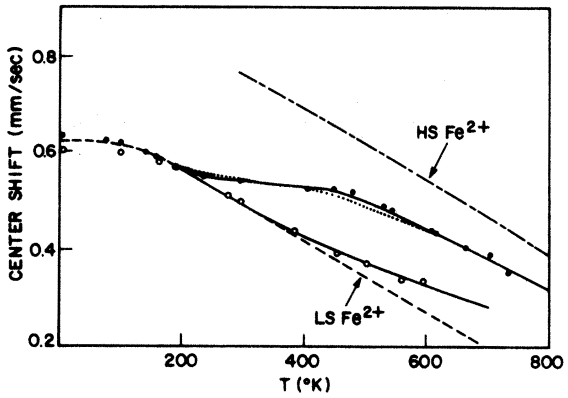

FIG. 6. Center shift of the Mössbauer absorption γ ray of ^{57}Fe in $1T$-$Fe_{0.1}Ta_{0.9}S_2$ expressed relative to metallic iron at 296 °K (dots). The open circles are δ_S for $Fe_{1/3}Ta_{2/3}S_2$. The dashed curve is the (assumed) second-order Doppler shift for low-spin Fe^{2+}. The full curves are the best-fit theory from Sec. VI using $k = 0.5$, $\delta/k|\Delta_0| = -1$, and the E_g data of Fig. 12. The implied high-spin Fe^{2+} SOD curve of Eq. (8) is shown by the point-dashed curve for $x = 0.1$. The dotted curve is the best-fit theoretical curve for $x = 0.1$ obtainable with a temperature-independent energy gap.

most unlikely situation. In general one would expect that the valence of Fe in a sulfide would be 3+ at most, the only other possibility being 2+. In the octahedrally coordinated substitutional (Ta) site there are accordingly only four possible magnetic states, viz., LS Fe^{2+} ($S=0$), HS Fe^{2+} ($S=2$), LS Fe^{3+} ($S=\frac{1}{2}$), and HS Fe^{3+} ($S=\frac{5}{2}$). Clearly the low temperature state is LS Fe^{2+}.

As the temperature is raised the susceptibility data show that a magnetic moment develops which at the highest temperatures measured has reached a value of $(4-5)\mu_B$. This can be qualitatively understood as a thermal population of higher-energy HS Fe^{2+} levels (with magnetic moment $\approx 4.9\mu_B$ for $g=2$, and larger if orbital contributions are significant) or as a thermal excitation of the sixth Fe^{2+} electron into the Ta conduction d band leaving behind high-spin Fe^{3+} (with magnetic moment $\approx 5.9\mu_B$), or possibly as a combination of both. An additional complication expected for any attempt at quantitative interpretation is the possible presence of a temperature-dependent Pauli paramagnetic contribution from the d-band conduction electrons themselves.

A number of these uncertainties can be resolved merely by plotting the susceptibility data of Fig. 1 in the form χT vs T^{-1} as shown in Fig. 7. If the dominant effect of increased temperature is a thermal excitation of Fe^{2+} electrons to the Ta d band then we expect χ as $T^{-1} \to 0$ to approach a value characteristic of Fe^{3+}. Neglecting for the moment possible Pauli complications we find, using $S=\frac{5}{2}$ and orbital angular momentum $L=0$ (i.e., $g=2$), a value $(\chi T)_{T\to\infty} = 4.374$ emu °K/mole. If the dominant thermal effect is an intraion excitation from LS to HS Fe^{2+} then, by virtue of the much higher multiplicity of the HS levels, we anticipate that the value of χT as $T \to \infty$ should closely approach that appropriate for HS Fe^{2+}. This is a little more difficult to calculate (since it depends on the effects of orbital angular momentum which is not quenched in HS Fe^{2+}) and may vary between ≈ 3.0 and 3.3 emu °K/mole, depending on the precise symmetry and covalency of the Fe in the Ta site (see below for details).

From Fig. 7 we see that the higher-temperature χT curves for $x=0.1$ to $\frac{1}{3}$ extrapolate rather convincingly to the HS Fe^{2+} alternative. This has two important implications: (a) that the dominant effect leading to the existence of a high-temperature magnetic moment is the thermal activation of the LS-HS Fe^{2+} transition and (b) that Pauli contributions (which would cause the curves to extrapolate to higher values of the ordinate) are essentially absent for iron concentrations in excess of $x=0.1$. The latter is presumably correlated with the large increase in resistivity resulting from iron doping. The $x=0.05$ curve in Fig. 7, which at first sight seems anomalous, can now be understood in terms of the existence of a Pauli contribution of non-negligible proportions in this the most electrically conductive of the iron-doped samples. To bring the $x=0.05$ curve into qualitative accord with the others (see Fig. 7) requires a Pauli contribution which increases with increas-

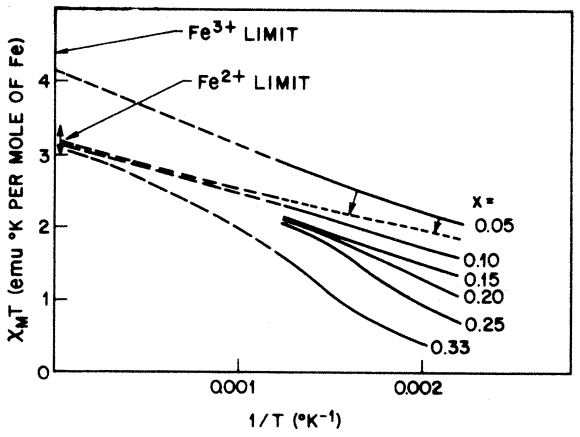

FIG. 7. Higher-temperature susceptibility data from Fig. 1 replotted as $\chi_m T$ vs $1/T$ and extrapolated to infinite temperature. On the ordinate we show the limiting values expected for Fe^{3+} high spin and Fe^{2+} HS (see text). The proposed shift of the $x=0.05$ curve on subtraction of a Pauli term (see text) is denoted by arrows.

ing T and reaches a value $\sim 0.13 \times 10^6$ emu/g at the highest temperatures observed ($\approx 800\,^\circ$K). This can be compared with the measured susceptibility[11] of $1T$-TaS_2 itself which reaches values $\sim 0.2 \times 10^6$ emu/g at higher temperatures. Since resistivity appears to increase monotonically with concentration x for fixed T, and monotonically with decreasing T for fixed x, this Pauli estimate for $1T$-$Fe_{0.05}Ta_{0.95}S_2$ is certainly not physically unreasonable. Since the addition of small amounts of substitutional impurity[13] rapidly removes the quasicommensurate and commensurate CDW instabilities responsible for the discontinuities evident in the TaS_2 susceptibility curve,[11] similar discontinuities are not anticipated for the $x = 0.05$ curve.

With this explanation of the $x = 0.05$ curve of Fig. 7 it is apparent that no evidence for the existence of Fe^{3+} can be found at any Fe concentration in the temperature range studied. It would therefore seem safe to attempt a quantitative analysis in terms of a LS-HS Fe^{2+} model.

V. LOW-SPIN–HIGH-SPIN STATISTICAL THEORY

We now consider a model in which each ferrous ion has a singlet $^1A_1$ ground state separated by an energy gap E_g from the lowest of the crystal-field and spin-orbitally-split HS states. We first consider the HS splitting as a separate problem. The statistical modification required in order to include the lone-singlet ground state of LS Fe^{2+} is minor and can be performed later.

The Fe^{2+} ion in $1T$-$Fe_xTa_{1-x}S_2$ sits at a trigonally distorted octahedral (Ta) site, with local symmetry $\bar{3}$. In a weak-field coupling scheme this term is split by the cubic part of the (sulfur-ligand) crystal field into an upper ^5E orbital doublet and a lower $^5T_2$ orbital triplet, separated by an energy gap $10Dq \sim 2 \times 10^4\,^\circ$K. From a statistical point of view the doublet can be neglected by virtue of its high energy. Within the triplet we can make use of the structural isomorphism of the T_2 and P symmetry groups to define a fictitious orbital angular momentum $L' = 1$. Within the levels of T_2 the matrix elements of real orbital angular momentum L are -1 times the equivalent elements of L' within the P states, while the matrix elements of L_z^2 are three times those of $L_z'^2$.

Labeling the threefold-symmetry axis at the Fe site as the z axis, we can write a Hamiltonian including a trigonal crystal-field distortion from cubic, a spin-orbit coupling term, and an applied field (H) energy, in the form

$$\mathcal{H} = \delta_0(L_z^2 - 2) + \lambda_0 \vec{L} \cdot \vec{S} - \mu_B(\vec{L} + 2\vec{S}) \cdot \vec{H}, \qquad (1)$$

in which δ_0 is a trigonal crystal-field energy parameter, $\lambda_0 = -103$ cm^{-1} is the spin-orbit-coupling constant for iron, and μ_B is the Bohr magneton. In a quasicubic crystal-field environment it is conventional to approximate the effects of covalency on the free-ion d orbitals by introducing a simple scalar orbital reduction parameter $k < 1$ acting on the orbital angular momentum operator viz., $\vec{L} \to k\vec{L}$. Using this notation and transforming to the fictitious orbital angular momentum representation we obtain

$$\mathcal{H} = \delta(L_z'^2 - \tfrac{2}{3}) + k|\lambda_0|\vec{L}' \cdot \vec{S} - \mu_B(2\vec{S} - k\vec{L}') \cdot \vec{H}, \qquad (2)$$

where $\delta = 3k^2\delta_0$ and we have dropped constant terms.

This Hamiltonian is readily diagonalized for $H = 0$ numerically within the basis states $|L_z', S_z\rangle$. The 15-fold-degenerate $^5T_2$ manifold ($L' = 1$, $S = 2$) is split into 6 doublets and 3 singlets.[21] For $1T$-$Fe_xTa_{1-x}S_2$ the sign of δ (and hence of $\delta/k|\lambda_0|$) is known from the Mössbauer quadrupole splitting to be reported in a separate paper—it is negative (i.e., with a doublet state lowest).

Having diagonalized (2) with $H = 0$ and obtained numerically the eigenfunctions and eigenvalues of the 15 HS states, zero-field HS statistical properties such as the partition function Z_{HS} and ensemble average $\langle L_z^2 - 2\rangle_{HS}$ or equivalently $\langle L_z'^2 - \frac{2}{3}\rangle_{HS}$ (which is required for a calculation of quadrupole splitting) are readily computed, assuming a Boltzmann distribution of energy levels, as functions of k and $\delta/k|\lambda_0|$. Moreover, perturbing the levels by an infinitesimal field term $-\mu_B(2\vec{S} - k\vec{L}') \cdot \vec{H}$ enables the components of zero-field magnetic susceptibility in the HS state χ_{HS}^i ($i = x, y, z$) and in particular the powder average $\chi_{HS} = 3^{-1}(\Sigma_i \chi_{HS}^i)$ to be computed in a straightforward manner, also as functions of k and $\delta/k|\lambda_0|$. In detail we have for the ith component of high-spin magnetic susceptibility per spin, ignoring the presence of interspin coupling,

$$kT\chi_{HS}^i = \sum_n \rho_n \left(\mu_{nn}^i \mu_{nn}^i + 2kT \sum_{m \neq n} \frac{\mu_{mn}^i \mu_{nm}^i}{(E_m - E_n)} \right), \qquad (3)$$

in which μ_{nm}^i is the matrix element of the ith component of magnetic moment $\vec{\mu} = \mu_B(2\vec{S} - k\vec{L}')$ between the nth and mth eigenstates of the ($H = 0$) zero-field energies, and ρ_n is the density matrix $e^{-E_n/kT}/Z_{HS}$, where

$$Z_{HS} = \sum_n e^{-E_n/kT}, \qquad (4)$$

is the partition function for the high-spin levels. Perhaps not surprisingly the powder average values are found to be roughly of Curie-law form, but with a Curie constant which, in addition to a

small temperature dependence, varies both with orbital reduction and trigonal distortion. Orbital reduction effects in Fe^{2+} systems are typically found to be of order $0.5 \lesssim k \lesssim 1$. Computing from (3), we show the temperature dependence of Curie constant $C = \chi_{HS} T$ for $k = 0.5$ and $k = 1.0$ and for the extremes $\delta/\lambda = 0$ and $-\infty (\lambda = k|\lambda_0|)$ of anisotropy in Fig. 8. In the infinite-temperature limit we find that the possible range of Curie values is rather small, viz., ~3.03–3.26.

To this point we have described calculations only for the HS ensemble. If the lowest of the HS levels actually sits at an energy E_g above a $^1A_1$ singlet ground state then the summation in (3) should be extended to include this state. Since there are no nonzero matrix elements of magnetic moment μ between the LS singlet and the HS levels, the new extended summation is readily transformed to a form explicitly involving only E_g and HS properties alone. We find specificially that the powder susceptibility for the LS-HS system takes the form

$$\chi = Z_{HS}(Z_{HS} + e^{E_g/kT})^{-1}\chi_{HS} . \quad (5)$$

It is now apparent that in the high-temperature limit ($Z_{HS} - 15$) the LS-HS susceptibility should actually tend toward $\frac{15}{16}\chi_{HS}$, some 6% lower than the limit shown in Fig. 7.

VI. ANALYSIS OF THE DATA

From Eqs. (3) and (5) it is evident that the LS-HS model is indeed in qualitative accord with the experimental susceptibility data of Fig. (1), but the measurements are in fact not quantitatively explained if the energy gap E_g is completely independent of temperature. A typical "best fit" to the data using a constant-gap model is shown for concentration $x = 0.1$ in Fig. 9. From this figure it is apparent that a quantitative fit would require

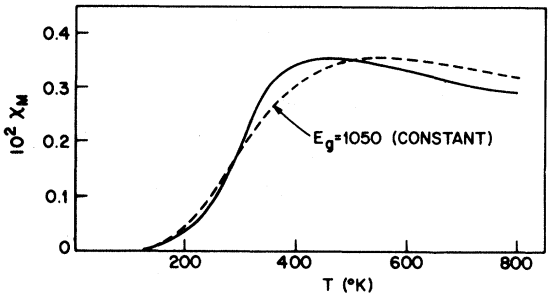

FIG. 9. Magnetic susceptibility per mole of iron for $Fe_{0.1}Ta_{0.9}S_2$ (full curve) from Fig. 1 versus temperature. The best-fit theoretical susceptibility curve obtainable using a temperature-independent energy gap $E_g = 1050$ °K is shown dashed.

a smaller (than average) gap at intermediate temperatures (300–500 °K) and a larger gap at both low and high temperatures. We now *define* a temperature-dependent gap $E_g(T)$ such that the theory of Eqs. (3) and (5) agrees exactly with experiment for magnetic susceptibility. However, since values for orbital reduction k and anisotropy δ/λ have not yet been determined, the resulting gap $E_g(T)$ is also, for the moment at least, a function of these parameters. In Fig. 10 we show $E_g(T)$ for $x = 0.1$ for various values of k and δ/λ. It is clear that the gap is "well-defined" to within an accuracy of about ±20% even in the absence of a knowledge of k and δ/λ, but that any detailed analysis of its temperature dependence cannot be attempted until some parameter estimates have been obtained. This can be accomplished by analyzing the Mössbauer data.

The center shift of the Mössbauer spectrum (Fig. 6) is the sum of an (essentially temperature independent) isomer shift (IS) and a temperature-dependent second-order Doppler shift (SOD). The IS is a measure of the S-electron charge density

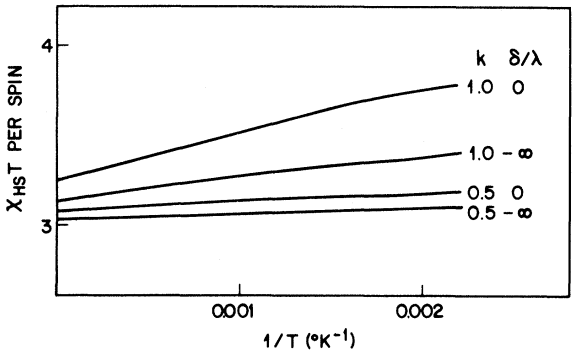

FIG. 8. Temperature dependence of Curie constant $C = \chi_{HS} T$ calculated from Eq. (3) versus $1/T$ for $k = 0.5$ and 1.0, and for the possible extremes $\delta/\lambda = 0$ and $-\infty$ of anisotropy ($\lambda = k|\lambda_0|$).

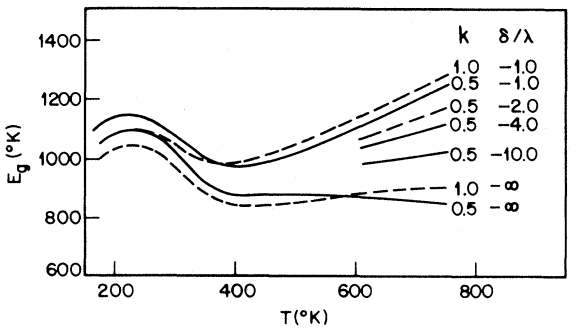

FIG. 10. Temperature dependence of the energy gap E_g calculated from Eqs. (3) and (5) to agree exactly with experimental χ for $x = 0.1$, the calculation being performed for various values of k and δ/λ.

at the ^{57}Fe nucleus,[22] while the SOD shift is produced by the thermal motion,[23] and is expected to be essentially the same for both HS and LS magnetic states. Its precise form ("thermal red shift") depends at low temperatures on the detailed phonon spectrum of the material, but at temperatures $T \gtrsim \Theta_D$ (Θ_D is the Debye temperature) the temperature dependence rapidly approaches a linear form with slope $3k/2Mc = 7.3 \times 10^{-4}$ mm/sec. We shall symbolize the SOD contribution to center shift as $(\delta_S)_{SOD}$ and assume it to be independent of HS-LS characterization. The IS contribution to center shift $(\delta_S)_{IS}$, though temperature independent, is a sensitive function of electron configuration with a HS value typically 0.3–0.4 mm/sec larger than a LS value. Therefore we write

$$\begin{aligned}(\delta_S)^{HS} &= (\delta_S)_{SOD} + (\delta_S)^{HS}_{IS}\,,\\ (\delta_S)^{LS} &= (\delta_S)_{SOD} + (\delta_S)^{LS}_{IS}\,,\\ (\delta_S)^{HS} - (\delta_S)^{LS} &= (\delta_S)^{HS}_{IS} - (\delta_S)^{LS}_{IS} = K \approx \text{const.}\end{aligned} \tag{6}$$

For the LS-HS situation of present interest the system therefore develops with temperature in a manner simply determined by the partition function of the levels, i.e.,

$$\delta_S = \frac{(\delta_S)^{LS} + Z_{HS}(\delta_S)^{HS} e^{-E_g/kT}}{1 + Z_{HS} e^{-E_g/kT}}\,, \tag{7}$$

which is more simply expressed in the form

$$\delta_S - (\delta_S)^{LS} = KZ_{HS}/(Z_{HS} + e^{E_g/kT})\,. \tag{8}$$

Assuming $(\delta_S)^{LS}$ to be a Debye SOD form (adjusted arbitrarily to fit the low-temperature data and extrapolated to its classical limiting linear form for $T \gtrsim 200\,^\circ$K) we now attempt to fit the $x = 0.1$ and $x = 0.33$ center-shift data of Fig. 6 using the approximate energy-gap values $E_g \approx 1000\,^\circ$K ($x = 0.1$) and $E_g \approx 2100\,^\circ$K ($x = 0.33$) with K, k, and δ/λ as variables.

Acceptable fits can only be obtained for smaller values of anisotropy ($|\delta/\lambda| \lesssim 4$) and for values of orbital reduction $k = 0.5 \pm 0.15$. A more precise measure of anisotropy can be obtained from the Mössbauer quadrupole splitting (to be reported in a separate paper) which establishes that δ/λ is certainly between -0.7 and -3.0 and probably between -1.0 and -1.5. Since the δ_S data are virtually insensitive to an anisotropy uncertainty of this order we have arbitrarily used the value $\delta/\lambda = -1$ for subsequent calculations. Shown in Fig. 6 are the best-fit constant-E_g theoretical curves from Eq. (8) for $x = 0.1$ and $x = 0.33$ ($k = 0.5$, $E_g = 1000$ and $2100\,^\circ$K, respectively, and $K = 0.25$ mm/sec.). As with the earlier constant-E_g susceptibility fit the theory is quite good but, for $x = 0.1$ in particular, not really quantitative. We now replot the $x = 0.1$ best-fit theoretical curve using, instead of a constant $E_g = 1000\,^\circ$K, that detailed temperature dependent $E_g(T)$ predicted from Fig. 10 for $k = 0.5$, $\delta/\lambda = -1$. The result, as shown in Fig. 6, is to produce essentially a quantitative fit to to the experimental data within the error of measurement (with $K = 0.27$ mm/sec). The point-dash curve in Fig. 6 is the predicted HS Fe^{2+}. The room-temperature-calculated IS for HS Fe^{2+} of 0.77 mm/sec is in very good agreement with the measured HS Fe^{2+} of 0.78 ± 0.01 mm/sec in the analogous HS intercalated compound $2H$-Fe_xTaS_2.[24] Extrapolating the high-temperature SOD for HS Fe^{2+} to low temperature yields an IS at 4.2 °K of 0.94 mm/sec. This is in excellent agreement with the measured IS of 0.95 ± 0.01 mm/sec for intercalated HS Fe^{2+} for $Fe_{1/3}TaS_2$. The IS for HS Fe^{3+} in octahedral environment is well below the δ_S measured in $Fe_xTa_{1-x}S_2$ ($0.1 \leq x \leq \frac{1}{3}$). A value of 0.31 mm/sec for IS at 296 °K was obtained by Coey *et al.*[25] for Fe^{3+} (octahedral environment) in Fe_3S_4. Vaughan and Ridout[26] obtained for Fe_3S_4 an IS of 0.45 mm/sec at 4.2 °K.

These results confirm the temperature dependence of E_g to be a real effect and pose the question of its physical origin. However, before discussing the latter we now assume that k and δ/λ are at most weak functions of the concentration x, and with $k = 0.5$ $\delta/\lambda \approx -1$, proceed from the measured susceptibilities for $x = 0.15$, 0.2, 0.25, and 0.33, to establish the detailed temperature dependence of energy gap E_g for the other iron concentrations measured. The resulting curves of $E_g(T)$ vs T (together with the relevant one for $x = 0.1$ from Fig. 10) are shown in Fig. 11. We have not included a curve for $x = 0.05$ because of the

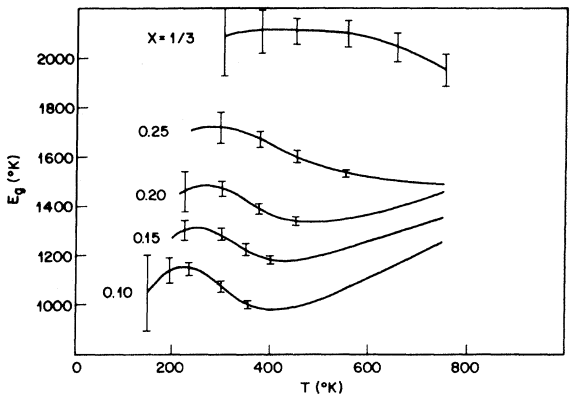

FIG. 11. Temperature dependence of energy gap E_g (for various values of Fe concentration x) as calculated by quantitatively fitting the χ data of Fig. 1 with $k = 0.5$ at $\delta/\lambda = -1$. No curve for $x = 0.05$ is shown because of the uncertainty of the magnitude of the Pauli concentration for this case (see text).

uncertainties introduced by the necessity of subtracting a Pauli susceptibility term for this case. It is evident that the gap E_g increases monotonically with concentration x and that the detailed form of the T dependence is modified as x increases, particularly for concentrations $x \gtrsim 0.2$. At first sight one might suspect that the (theoretically neglected) exchange interactions between iron spins might be upsetting the details for the larger iron concentrations, but we shall later demonstrate that the major development of $E_g(T)$-curve shape with increasing concentration x is a real single-ion effect and that accordingly exchange interactions do not seem to produce any significant effects in the present experiments. It is important to note that $E_g(T)$ never approaches zero (i.e, a true cross crossover) so that the LS-HS "transition" occurs as a function of increasing temperature in a statistical sense only by virtue of the much higher degeneracy of the higher-energy (HS) state.

Since the ionic radius of Fe^{2+} ($S=2$) is larger than that of Fe^{2+} ($S=0$),[27] and the latter is smaller than Ta^{4+} or Ta^{5+}, we expect deviations from the usual linear thermal lattice expansion in the transition region. These have been observed. For example (at $x=0.20$) $(1/a)(da/dT)=5.4\times10^{-5}\,^{\circ}K^{-1}$ when $300<T<500\,^{\circ}K$, but for $T>580\,^{\circ}K$ $(1/a)(da/dT)=0.6\times10^{-5}\,^{\circ}K^{-1}$. The latter is rather typical of thermal expansion in layer compounds.[28] Also as x increases the hexagonal unit-cell volume decreases (for example, $\Delta V/V$ at 295 °K when x increases from 0.1 to 0.2 is −0.70%). This decrease may in part be due to a decrease in Fe–S bond length, increasing the cubic crystal field. Thus a larger lattice expansion (higher temperature) would be necessary to reach the crossover condition at higher x concentrations. This possibility is consistent with the observation in Fig. 1 that the transition to the high-spin state moves to higher temperatures with increasing x.

In $1T$-TaS_2 the peak-to-peak CDW amplitude in the the conduction-band charge density becomes as large as one electron per atom at low temperatures.[29] Such large changes in the charge distribution, expected at least at low x, could affect the magnitude of the crystal field. Thus, indirectly the CDW may play a role in the LS-HS transition.

We conclude, therefore, from this section, that the iron is indeed in a ferrous form throughout, that a $^1A_1$ low-spin state is the ground-energy state at all temperatures, and that the energy gap E_g separating the lowest of the excited levels from the ground state is ~1000 °K for $x=0.1$ increasing to ~2100 °K for $x=0.33$. Most importantly the gap E_g is temperature dependent for each concentration exhibiting (in general) first a maximum and then a minimum as a function of increasing temperature with $\Delta E_g = E_g(\max) - E_g(\min)$ of order 200 °K. The orbital reduction factor $k=0.5\pm0.15$ indicates extreme covalency, a finding which is also confirmed by the Mössbauer quadrupole data to be reported in a separate paper.

VII. ORIGIN OF THE GAP TEMPERATURE DEPENDENCE

The energy gap $E_g(T)$ is defined as the energy separation of the LS singlet ground state and the *lowest* of the HS $^5T_2$ states. The energy separation of the LS ground state and the "center of gravity" of the $^5T_2$ levels (i.e., the position of the fully degenerate $^5T_2$ level in the absence of spin-orbit and trigonal field perturbations) can be expressed simply as the difference $20Dq - E_H$ between the cubic crystal-field energy required to promote two d electrons from t_2- to e-symmetry single-electron orbitals ($20Dq$) and the Hund's-rule exchange energy E_H gained by flipping spins of the two promoted electrons. For a doublet ground state we can write[21]

$$E_g = 20Dq - E_H - 3k|\lambda_0| - \delta E(\text{trig}), \tag{9}$$

in which the final term is the small energy perturbation of the ground HS level produced by the trigonal field term $\delta(L_z'^2 - \frac{2}{3})$ in Eq. (2), For $k=0.5$, $\delta/\lambda=-1$ ($\lambda=k|\lambda_0|$), we find values $3k|\lambda_0| \sim 220\,^{\circ}K$ and $\delta E(\text{trig}) \sim 10\,^{\circ}K$ so that the established temperature variations in $E_g(T)$ of order 200 °K cannot result from any small temperature dependence of covalency (i.e., orbital reduction) or even large variations of trigonal distortion. It follows that the physical origin of this effect must reside in a temperature dependence of $20Dq$ or E_H, or both. Since $20Dq \sim E_H \approx (3-4)\times10^4\,^{\circ}K$ the observed temperature dependence of E_g amounts to only a fraction of 1% of these energies and could therefore be readily accounted for by a small environmental dependence or either or both.

The most likely origin is a modulation by a local "breathing mode" ligand vibration. Although it would seem physically more likely for the modulation of $20Dq$ to be dominant (since E_H is an intraion property) we can allow for either by simply expanding $\Delta = 20Dq - E_H$ at an arbitrary lth site as a function of a local harmonic ligand displacement coordinate ξ_l to second order, i.e.

$$\Delta_l = \Delta - \Delta'\xi_l + \tfrac{1}{2}\Delta''\xi_l^2, \tag{10}$$

where $\Delta=\Delta_l$ ($\xi_l=0$), $\Delta'=\partial\Delta_l/\partial\xi_l$ at $\xi_l=0$, and $\Delta''=\partial^2\Delta_l/\partial\xi_l^2$ also evaluated at $\xi_l=0$. Arbitrarily choosing the LS $^1A_1$ electronic level as our zero of energy we can now write local (lth site) LS and HS Hamiltonians, including the vibrational potential term, as

$$\mathcal{H}_l^{\mathrm{HS}} = \Delta - \Delta' \xi_l + \tfrac{1}{2}\Delta'' \xi_l^2 + \delta(L_z'^2 - \tfrac{2}{3}) + \lambda \vec{L}' \cdot \vec{S} + \tfrac{1}{2}\Omega^2 \xi_l^2 , \quad (11)$$

$$\mathcal{H}_l^{\mathrm{LS}} = \tfrac{1}{2}\Omega^2 \xi_l^2 ,$$

where Ω is the frequency of the relevant local mode of vibration. Expanding about the equilibrium position $Q = \langle \xi_l \rangle$ and ensemble averaging over the lattice coordinates ξ_l we obtain the effective "magnetic" Hamiltonians

$$\mathcal{H}^{\mathrm{HS}} = \Delta - \Delta' Q + \tfrac{1}{2}(\Delta'' + \Omega^2)[\langle (\xi_l - Q)^2 \rangle + Q^2] + \delta(L_z'^2 - \tfrac{2}{3}) + \lambda \vec{L}' \cdot \vec{S} \quad (12)$$

$$\mathcal{H}^{\mathrm{LS}} = \tfrac{1}{2}\Omega^2[\langle (\xi_l - Q)^2 \rangle + Q^2] ,$$

with eigenvalues E_i^{HS} and E^{LS}, respectively. It follows that

$$E_g(T) = \Delta_0 - \Delta' Q + \tfrac{1}{2}\Delta''[\langle (\xi_l - Q)^2 \rangle + Q^2] , \quad (13)$$

where $\Delta_0 = \Delta - 3\lambda - \delta E(\mathrm{trig}) \approx \Delta - 230\,^\circ\mathrm{K}$, for our case. Thus, the gap consists of a static part $E(\mathrm{stat}) = \Delta_0 - \Delta' Q + \frac{1}{2}\Delta'' Q^2$ and a "dynamic" part $E(\mathrm{dyn}) = \frac{1}{2}\Delta''\langle (\xi_l - Q)^2 \rangle$. Since the root-mean-square amplitude of vibration is almost certainly large compared with static displacement Q, it is likely that the dynamic term is essentially independent of Q and this we shall assume. The thermal equilibrium displacement Q is now obtained by minimizing the free energy per ferrous ion

$$F = \sum_i [(E_i^{\mathrm{HS}} - E^{\mathrm{LS}}) n_i + E^{\mathrm{LS}}] , \quad (14)$$

where n_i is an ensemble-averaged occupation number for the ith HS energy level, with respect to Q. Explicitly this can be written

$$F = \tfrac{1}{2}\Omega^2[\langle (\xi - Q)^2 \rangle + Q^2] - kT \ln(1 + e^{-(E_g + E_i)/kT}) , \quad (15)$$

in which i runs over the 15 HS levels and E_i is now measured from the bottom of the HS multiplet. Minimizing with respect to Q we find the condition

$$\Omega^2 Q(Z_{\mathrm{HS}} + e^{E_g/kT}) = Z_{\mathrm{HS}}(\Delta' - Q\Delta'') , \quad (16)$$

where Z_{HS} and E_g are given by (4) and (13), respectively. Finally, the ensemble average $\langle (\xi_l - Q)^2 \rangle$ is given in a simple harmonic approximation by the standard quantum form $(\hbar/2\Omega)\coth(\hbar\Omega/2kT)$ in terms of which the "dynamic" contribution to $E_g(T)$ can be expressed as

$$E(\mathrm{dyn}) = \tfrac{1}{2}\Delta''\langle (\xi_l - Q)^2 \rangle = (\hbar\Delta''/4\Omega)\coth(\hbar\Omega/2kT) . \quad (17)$$

Equations (13), (16), and (17) now form a self-consistent set for the theoretical determination of the energy gap as a function of temperature. The energy levels E_i^{HS} can be taken as known (using $k = 0.5$, $\delta/\lambda = -1$) so that the available parameters are Δ_0, Δ', Δ'', and the local mode frequency Ω. However, since we are not able to determine the "experimental" $E_g(T)$ of Fig. 11 with any accuracy for temperatures below $T \lesssim 200\,^\circ\mathrm{K}$, and the dynamic contribution (17) rapidly becomes linear in T (with slope $\frac{1}{2}k\Delta''/\Omega^2$) as T increases beyond $\sim \hbar\Omega/2k$, it turns out that the temperature variation of E_g as we know it (i.e., between about 200 and 800 °K) is essentially dominated by only three parameters Δ_0, Δ'^2/Ω^2, and Δ''/Ω^2. For example, the static energy gap can be rewritten as an expansion in the energy parameter $\Delta' Q$ in the form

$$E_g(\mathrm{stat}) = \Delta_0 - \Delta' Q + \tfrac{1}{2}(\Delta''/\Omega^2)(\Omega^2/\Delta'^2)(\Delta' Q)^2 , \quad (18)$$

where $\Delta' Q$ is given directly from (16) as

$$\Delta' Q = f(\Delta'^2/\Omega^2)/[1 + f(\Delta''/\Omega^2)] , \quad (19)$$

in which

$$f = Z_{\mathrm{HS}}/(Z_{\mathrm{HS}} + e^{E_g/kT}) \quad (20)$$

and

$$E_g = E_g(\mathrm{stat}) + E_g(\mathrm{dyn}) . \quad (21)$$

Absorbing any zero-point dynamic contribution (i.e., $\hbar\Delta''/4\Omega$) into the parameter Δ_0, self-consistent solutions of (17)–(21) have been obtained numerically for E_g as a function of T, using Δ_0, Δ'^2/Ω^2, and Δ''/Ω^2 as parameters, and fitted to the "experimental" data of Fig. 11. The resulting best fits to the data are shown in Fig. 12 for all concentrations $x = 0.1$–0.33. The actual computations have been performed setting $\hbar\Omega = 200\,^\circ\mathrm{K}$ although essentially equivalent fits can be obtained

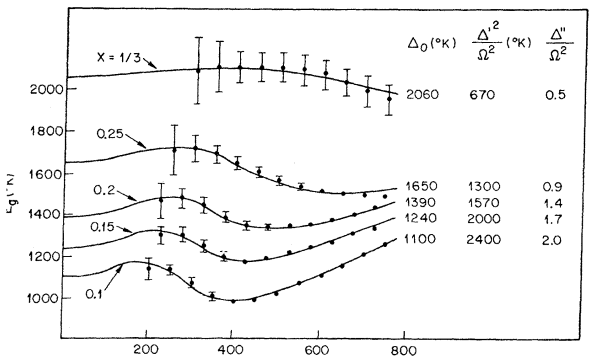

FIG. 12. Filled circles and error bars indicate the temperature dependence of the energy gap E_g (for various values of Fe concentration x) as taken from Fig. 11. The continuous curves are calculated directly from the lattice phonon modulation theory of the text. The relevant values of the three defining parameters of that theory, namely, Δ_0, Δ'^2/Ω^2, and Δ''/Ω^2 are given for each concentration and show a monotonic variation with x.

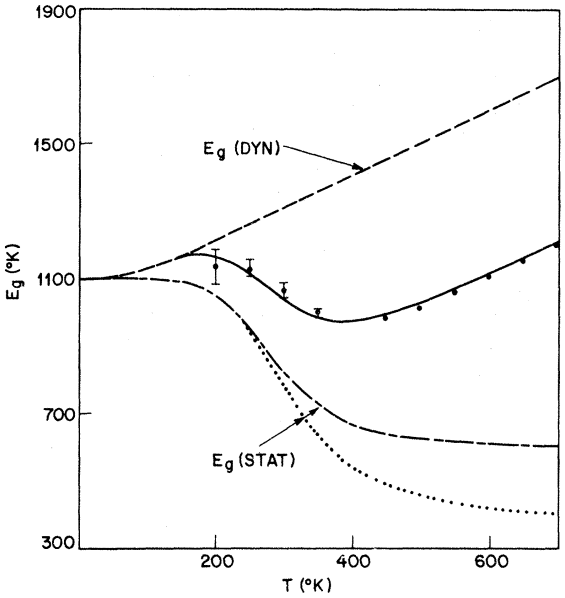

FIG. 13. Filled circles and error bars indicate the "experimental" temperature dependence of the energy gap E_g for $x=0.1$ as in Fig. 12. The dotted curve is the first-order static, the dot-dashed curve the sum of the first- and second-order static, and the dashed curve the dynamic contribution to the energy gap E_g as calculated from Eqs. (17) and (18) of the text. The full curve is the sum of the total static (dot-dashed) and dynamic (dashed) contributions to E_g.

with $\Omega = 400\ °K/\hbar$ or even higher with minor compensating adjustments of Δ_0. We find that the temperature dependence of the gap can be quantitatively explained for all five concentrations $x=0.1$, 0.15, 0.2, 0.25, 0.33 with each of the three relevant parameters Δ_0, Δ'^2/Ω^2, and Δ''/Ω^2 varying monotonically with concentration as shown in Fig. 12. The manner in which the first- and second-order static contributions of Eq. (18) and the dynamic contribution of Eq. (17) sum to give the final resultant $E_g(T)$ is shown in Fig. 13. We see that the dynamic term dominates the temperature dependence at both low and high temperatures with the static "striction" anomaly dominating at intermediate temperatures. Although the best-fit parameter values given in Fig. 12 provide, in view of our almost complete lack of knowledge of local mode frequency Ω, a less than complete picture, they do show a rough proportionality of Δ'^2/Ω^2 and Δ''/Ω^2 as functions of x. This suggests that the most concentration dependent of the fundamental physical quantities involved is probably the local mode frequency itself. The whole picture is then explicable in terms of very weakly concentration-dependent crystal-field and Hund's-rule energies (and their strain dependencies) and a local mode frequency which increases by close to a factor of 2 as the concentration x increases from 0.1 to 0.33. The important concentration dependence of Δ_0 results of course only from the accidental near equality of $20Dq$ and E_H is this particular material.

ACKNOWLEDGMENTS

We thank M. Robbins for reducing $^{57}Fe_2O_3$ in ^{57}Fe metal and J. V. Waszczak for technical assistance. We are grateful to M. D. Sturge, G. K. Wertheim, J. A. Wilson, and Y. Yafet for helpful discussions.

[1]R. R. Heikes, R. C. Miller, and R. Mazelsky, Physica 30, 1600 (1964).
[2]P. M. Raccah and J. B. Goodenough, Phys. Rev. 155, 932 (1967).
[3]E. Konig and K. Madeja, Inorg. Chem. 6, 48 (1967).
[4]E. Konig, K. Madeja, and K. J. Watson, J. Am. Chem. Soc. 90, 1146 (1968).
[5]R. J. Dosser, W. J. Eilbeck, A. E. Underhill, P. R. Edwards, and C. E. Johnson, J. Chem. Soc. A 5, 810 (1969).
[6]E. Konig, G. Ritter, H. Spiering, S. Kremer, K. Madeja A. Rosenkrantz, J. Chem. Phys. 56, 3139 (1972); E. Konig and G. Ritter, In *Mossbauer Effect Methodology*, edited by I. J. Gruvermann (Plenum, New York, 1973), Vol. 9, p. 3.
[7]R. A. Bari and J. Sivardière, Phys. Rev. B 5, 4466 (1972).
[8]D. B. Chestnut, J. Chem. Phys. 40, 405 (1964).
[9]M. Eibschütz and F. DiSalvo, Phys. Rev. Lett. 36, 104 (1976).
[10]M. E. Lines and M. Eibschütz, J. Phys. C 9, L355 (1976).
[11]J. A. Wilson, F. J. DiSalvo, and S. Mahajan, Advan. Phys. 24, 117 (1975).
[12]F. J. DiSalvo, B. G. Bagley, J. M. Voorhoeve, and J. V. Waszczak, J. Phys. Chem. Solids 34, 1357 (1973).
[13]F. J. DiSalvo, J. A. Wilson, B. G. Bagley, and J. V. Waszczak, Phys. Rev. B 12, 2220 (1975).
[14]R. M. Fleming and R. V. Coleman, Phys. Rev. Lett. 34, 1502 (1975).
[15]F. J. DiSalvo, M. Eibschütz, J. A. Wilson, and J. V. Waszczak, Bull. Am. Phys. Soc. 20, 290 (1975); M. Eibschütz and F. J. DiSalvo, *ibid.* 20, 289 (1975).
[16]W. L. McMillan, Phys. Rev. B 12, 1187 (1975).
[17]R. L. Cohen, Rev. Sci. Instrum. 37, 260 (1966); 37, 957 (1966).
[18]G. R. Davidson, M. Eibschütz, and H. J. Guggenheim, Phys. Rev. B 8, 1864 (1973); M. Eibschütz, G. R. Davidson, and H. J. Guggenheim, *ibid.* 9, 3885 (1974).
[19]R. L. Cohen and G. K. Wertheim, in *Methods of Experimental Physics*, edited by R. V. Coleway (Academic, New York, 1974), Vol. II, Pt. 6, Fig. 16. The furnace was kindly loaned by G. K. Wertheim.

[20]N. M. Greenwood and T. C. Gibb, in *Mossbauer Spectroscopy* (Chapman and Hall, London, 1971), p. 91, Fig. 5.2.
[21]J. S. Griffith, in *The Theory of Transition-Metal Ions*, (Cambridge U. P., London, 1961), p. 357, Fig. 12.6.
[22]L. R. Walker, G. K. Wertheim, and V. Jaccarino, Phys. Rev. Lett. 6, 98 (1961).
[23]R. V. Pound and G. A. Rebka, Jr., Phys. Rev. Lett. 4, 274 (1960); B. D. Josephson, *ibid.* 4, 341 (1960).
[24]M. Eibschütz, F. J. DiSalvo, G. W. Hull, Jr. and S. Mahajan, Appl. Phys. Lett. 27, 464 (1975).
[25]J. M. D. Coey, M. R. Spender, and A. H. Morrish, Solid State Commun. 8, 1605 (1970).
[26]D. J. Vaughan and M. S. Ridout, J. Inorg. Nucl. Chem. 33, 741 (1971).
[27]R. D. Shannon and C. T. Prewitt, Acta Crystallogr. B 25, 946 (1969).
[28]M. S. Whittingham and A. H. Thomson, J. Chem. Phys. 62, 1588 (1975).
[29]G. K. Wertheim, F. J. DiSalvo, and S. Chiang, Phys. Lett. A 54, 304 (1975).